RSC Advances

PAPER

View Article Online
View Journal | View Issue

Check for updates

Cite this: *RSC Adv.*, 2021, **11**, 11295

Mechanistic insights into the C–H activation of methane mediated by the unsupported and silica-supported VO_2OH and CrOOH: a DFT study†

Shidong Zhao,‡[a] Lishuang Ma,‡[a] Yanyan Xi,[bc] Hongyan Shang*[ac] and Xufeng Lin *[ac]

The direct activation and conversion of methane has been a topic of interest in both academia and industry for several decades. Deep understanding of the corresponding mechanism and reactivity mediated by diverse catalytic clusters, as well as the supporting materials, is still highly desired. In this work, the regulation mechanism of C–H bond activation of methane, mediated by the closed-shell VO_2OH, the open-shell CrOOH, and their silica supported clusters, has been investigated by density functional theory (DFT) calculations. The hydrogen-atom transfer (HAT) reaction towards methane C–H bond activation is more feasible when mediated by the unsupported/silica-supported CrOOH clusters *versus* the VO_2OH clusters, due to the intrinsic spin density located on the terminal O_t atom. The proton-coupled electron transfer (PCET) pathways are regulated by both the nucleophilicity of the O_t site and the electrophilicity of the metal center, which show no obvious difference in energy consumption among the four reactions examined. Moreover, the introduction of a silica support can lead to subtle influences on the intermolecular interaction between the CH_4 molecule and the catalyst cluster, as well as the thermodynamics of the methane C–H activation.

Received 23rd December 2020
Accepted 5th March 2021

DOI: 10.1039/d0ra10785a

rsc.li/rsc-advances

Open Access Article. Published on 17 March 2021. Downloaded on 2/9/2026 10:09:49 PM.
This article is licensed under a Creative Commons Attribution-NonCommercial 3.0 Unported Licence.

1. Introduction

Methane (CH_4), as the major component of natural gas, is not only an important clean fuel, but also an abundant hydrocarbon feedstock for chemical commodities.[1,2] In the recent decades, with the development of modern catalytic technologies, the direct nonoxidative activation and conversion of methane to high value-added chemicals has received significant interest, from both industry and academia.[3–6] Although a variety of strategies have been developed, C–H bond activation, the first and also critical step for methane conversion is still challenging. This challenge arises from the fact that the extremely symmetric nonpolar methane molecule exhibits a high C–H bond dissociation energy (439 kJ mol^{-1}).[7,8] To avoid the high temperature and harsh reaction conditions, efficient catalysis under mild conditions as well as the deep understanding of the underlying mechanism for direct methane activation has always been highly desirable.[9–12]

Up to now, a great deal of effort has been devoted on the metal-cluster-mediated methane activation reactions, using both experimental and theoretical methods. These metal cluster species, including the metal oxide cluster,[13,14] metal carbides,[15,16] and metal cluster anions[17,18] *etc.*, can be regarded as simplified models of methane activation sites on heterogeneous catalysts. Meanwhile, the knowledge of the fundamental reaction mechanism towards the methane activation and conversion is continuously being improved.[13–18] For example, Sun *et al.* reported that the C–H bond activation may undergo a concerted pathway where the C and H atoms on the C–H bond attack two different sites, accompanied by formatting two new bonds (C–Ni and O–H), or a stepwise pathway where two separated products of Ni_3O_3H and ethyl radical can be obtained.[19] Wan *et al.* found that the terminal oxygens [=O] are more active than the bridge oxygens [–O–] for C–H bond activation of methane on molybdenum oxides.[20] Interestingly, the adsorbed oxygen species on metal surfaces were demonstrated to exhibit promotional or inhibitory effects, which depends strongly on the nature of metals.[21–26] In more recent years, a series of mechanistic scenarios were explored by Schwarz *et al.*,[13–16,27–29] in which the classical hydrogen-atom transfer (HAT),[27] proton-coupled electron transfer (PCET),[28] and hydride transfer (HT)[29] pathways were explored and distinguished in various reaction systems for methane C–H activation.

[a]*Department of Chemistry, College of Science, China University of Petroleum (East China), Qingdao, 266580, P. R. China. E-mail: catagroupsh@163.com; hatrick2009@upc.edu.cn*

[b]*College of Chemical Engineering, China University of Petroleum (East China), Qingdao, 266580, P. R. China*

[c]*State Key Laboratory of Heavy Oil Processing, China University of Petroleum (East China), Qingdao, 266580, P. R. China*

† Electronic supplementary information (ESI) available: The symmetry-adapted perturbation theory (SAPT) energy decomposition and Hirshfeld spin density and charge population analyses, and Cartesian coordinates of all optimized structures. See DOI: 10.1039/d0ra10785a

‡ These authors contributed equally to this work.

© 2021 The Author(s). Published by the Royal Society of Chemistry

Open Access Article. Published on 17 March 2021. Downloaded on 2/9/2026 10:09:49 PM.
This article is licensed under a Creative Commons Attribution-NonCommercial 3.0 Unported Licence.

Although significant progress has been made in methane activation mediated by metal clusters, the reported gas-phase atom clusters obtained by state-of-the-art mass spectrometric are generally ionic species.[13–20] While, researches on the catalytic activity of the neutral metal oxyhydroxide towards C–H bond activation of methane are still sparse. Typically, the earth abundant vanadium and chromium have been demonstrated good catalytic capability for C–H activation,[30–32] but few studies have focused on their neutral oxyhydroxides, such as VO_2OH and CrOOH. In addition, in industrial catalytic processes, catalyst supports are usually introduced to disperse and support active components, which can lead to a lower cost of the transition metal as well as a higher stability of the catalytic material compared with the unsupported ones.[33] However, detailed understanding of the support effect on catalyst activity, and the interaction between support and active components is yet to be more thoroughly investigated, especially at the molecular level.[33,34]

Herein, we report a theoretical study on C–H bond activation of methane mediated by the silica-supported/unsupported VO_2OH and CrOOH clusters, through the density functional theory (DFT) calculations. The HAT and PCET reaction channels were carefully examined to obtain a better understanding towards the catalytic activity of the closed-shell VO_2OH and the open-shell CrOOH, as well as the effect of silica support.

2. Computational methods

In the present study, DFT calculations were performed using the Gaussian 09 program package,[35] to investigate the reaction mechanism of methane activation catalyzed by the VO_2OH and CrOOH catalysts, as well as their silica-supported complexes, as shown in the following equations:

CH_4 + an unsupported VO_2OH cluster (i)

CH_4 + a model silica supported VO_2OH cluster (ii)

CH_4 + an unsupported CrOOH cluster (iii)

CH_4 + a model silica supported CrOOH cluster (iv)

In our calculations, a cluster containing $Si_4O_6H_3$ was used to model the silica support surface, denoted as "Sili" in this paper. All Si centers have a tetrahedron local structure simulating the SiO_4 tetrahedron moiety, and the H atoms were used to saturate the boundary dangling bonds of the Si centers. The VO_3@Sili and CrO_2@Sili were used to denote the complexes that the VO_3^- and CrO_2^- clusters supported on the silica model. In addition, a larger cluster models, $Si_{16}O_{30}H_3$, denoted as "Sili2", was used to investigate the cluster size effects (details can be seen from the Section 3.4), which showed that the smaller cluster model of $Si_4O_6H_3$ used in this article are as reliable as that with the larger one.

All minima of the reactants and the corresponding products for Rxn (i)–(iv) were first obtained by full system optimization, using the hybrid density functional[36–38] including empirical dispersion correction computed with Grimme's D3 formula (B3LYP-D3).[39] Note that the open-shell configurations were calculated within the spin-unrestricted approximation, in which the broken-symmetry technique was introduced to treat the singlet (Rxn (i) and (ii)) and quartet (Rxn (iii) and (iv)) radical HAT pathway. The energy-consistent scalar-relativistic DF-adjusted 10-electron-core pseudopotential/ECP10MDF(8s7p6d1f/6s5p3d1f) basis set was used for V and Cr,[40] while the def-TZVP[41,42] basis set was applied for all other atoms. The transition states (TSs) for C–H bond activation of CH_4 mediated by V and Cr catalysts were obtained by employing the conventional approach of transition state optimization. Based on the optimized geometries, vibrational frequency analyses were carried out at the same level of theory to ensure that each stationary point truly represented a minimum, or a saddle point, and to obtain the thermal enthalpy corrections at 298.15 K and 1 atm. Intrinsic reaction coordinate (IRC) computations[43,44] were also conducted to confirm that the transition states connected to the appropriate reactants and products. Finally, the electronic energies were refined with the B3LYP-D3 functional and a larger basis set, in which the DF-adjusted 10-electron-core pseudopotential/ECP10MDF(8s7p6d2f1g)/[6s5p3d2f1g] was used for V and Cr,[45] while the ma-def2-TZVPP[46,47] basis set was used for all other atoms. To reduce the unaffordable computational cost on reactions mediated by the larger cluster model, $Si_{16}O_{30}H_3$, the basis set for the reaction center was used as same as that smaller reaction models above, while a smaller def-SV basis set was applied to the remaining atoms away from the reaction center, the corresponding mixed basis set applied for the geometry optimization and frequency calculations is the denoted as BSI, and that used for the refined single-point-energy calculation is denoted as BSII (see Fig. S1†).

The charge and spin density populations analyses were performed by the Hirshfeld method.[48] The spin-density isosurfaces (isovalue 0.02) were plotted using a multifunctional wavefunction analyzer (Multiwfn).[49] The symmetry-adapted perturbation theory (SAPT) energy decomposition analysis was carried out at the SAPT0/def2-TZVPP level, by using PSI4 program package.[50] The total SAPT0 interaction energy (ΔE_{int}) between the CH_4 and the catalyst cluster can be decomposed into contributions of the electrostatic (ΔE_{els}), exchange-repulsion (ΔE_{exc}), induction (ΔE_{ind}) and dispersion (ΔE_{disp}) terms:

$$\Delta E_{tot} = \Delta E_{els} + \Delta E_{exc} + \Delta E_{ind} + \Delta E_{disp}$$

The notations having the form of [**R**/**TS**/**P**]-*n* will be used in the later sections, where **R**/**TS**/**P** represents the reactant, transition state or product, and *n* represents one of (i)–(iv) for the Rxn numbers defined above. Meanwhile a superscript will be used before a species name to represent the spin multiplicity of this species. For example, the ^{4}**TS$_{HAT}$-iv** denotes the quartet transition state of Rxn (iv) along the HAT pathway.

3. Results and discussion

3.1 Structures and properties of the unsupported/silica-supported VO_2OH and CrOOH clusters

The stable structures, charge and spin density properties of the unsupported and silica-supported VO_2OH and CrOOH clusters

© 2021 The Author(s). Published by the Royal Society of Chemistry

Open Access Article. Published on 17 March 2021. Downloaded on 2/9/2026 10:09:49 PM.
This article is licensed under a Creative Commons Attribution-NonCommercial 3.0 Unported Licence.

were investigated at first. As shown in Fig. 1, the free VO_2OH has two terminal oxygen atoms (O_t), which have the same V–O_t bond length of 1.59 Å and equivalent charge of $-0.31e$. The free CrOOH have one terminal O_t atom with $-0.36e$ charge and an O–H bond of length 1.59 Å. These calculations results show that both VO_2OH and CrOOH possess Lewis acid–base pair [M^{n+}(V^{5+}/Cr^{3+})–O^-] units,[28] facilitating the C–H bond activation through the PCET pathway. For the HAT mechanism for C–H activation, the O_t-center spin is necessary as the precursor state to abstract H atom.[51,52] Since the VO_2OH is closed-shell singlet, zero spin density were found on the O_t atom. By contrast, obvious spin density of -0.21 was observed located on the O_t atom of the open-shell CrOOH cluster, which is reasonable due to the Cr^{3+} is initially a quartet, with three unpaired electrons in the 3d orbitals. In consequence, the O_t site on CrOOH is expected to be more advantageous for a radical HAT reaction; whereas, for the O_t site on the closed-shell VO_2OH, an electron reorganization is needed to accumulate O-center spin density to trigger the radical HAT process, indicating a higher energy barrier should be overcome.

In the presence of the silica support, the hydroxyl groups of both VO_2OH and CrOOH have to deprotonate to combine with the Si atom through chemisorption, forming a new Si–O bond (1.62 Å). In this condition, slight structural change and charge reorganization were observed from our computational results. As shown in Fig. 1, the O_t atom is slightly less negatively charged upon silica support for both VO_3@Sili and CrO_2@Sili clusters [VO_2OH ($-0.31e$) → VO_3@Sili ($-0.29e$); CrOOH ($-0.36e$) → CrO_2@Sili ($-0.33e$)]. Besides the charge-regulation effect, the spin density on the O_t atom of CrOOH is a little increased upon silica support [CrOOH ($-0.21e$) → CrO_2@Sili ($-0.25e$)]. Since the methane C–H activation reaction is sensitive to the charge and spin density of the O_t atom, the silica support may lead to subtle influences on the potential energy profiles (PESs) of methane activation on the VO_2OH and CrOOH clusters. Details about the mechanism of the reactions Rxn (i)–(iv) will be discussed in the Sections 3.2 and 3.3. It should be noted that, the free CrOOH in doublet state was calculated energetically 16.4 kcal mol^{-1} higher than that in quartet state. It suggests that the electronic ground state is a quartet state with three parallel-spin electrons occupying three 3d orbitals ($t_{2g}^3e_g^0$). Thus, the doublet CrOOH were not considered in this work for the reactions Rxn (iii) and (iv).

3.2 Thermal activation of CH_4 on VO_2OH clusters

3.2.1 Rxn (i): reaction on an unsupported VO_2OH cluster. Fig. 2 shows the PESs of C–H activation of CH_4 on a VO_2OH cluster (Rxn (i)) as well as the related critical structures. Once the separated reactants CH_4 and VO_2OH encounter each other, an encounter reactant complex **^{1}EC-i** is formed with an energy decrease of 13.1 kcal mol^{-1}. The stabilization energy results mainly from the electrostatic and induction effects from the SAPT energy decomposition analysis (see Table S1 in the ESI†). The intermolecular interaction also leads to a charge transfer ($0.21e$) from the CH_4 moiety to the VO_2OH cluster (see Table S2 in the ESI†). Meanwhile, the CH_4 molecule is slightly polarized, that two C–H bonds facing the VO_2OH cluster are stretched from 1.09 Å to 1.10–1.11 Å. In this case, the CH_4 molecule is initially activated compare with its inherently nonpolar structure with four C–H bonds of equal length (1.09 Å) and zero dipole moment.

After **^{1}EC-i** is formed, one C–H bond of methane could be activated under two mechanisms in principle, that is, the HAT and the PCET mechanisms. As illustrated in Fig. 2, since the products of CH_4 activation *via* a radical HAT mechanism are two separated radicals, the open-shell singlet channel and triplet channel were both examined for the HAT mechanism. Population analyses results reveal that the electron reorganization is necessary to access the transition states **^{1}TS$_{HAT}$-i** or **^{3}TS$_{HAT}$-i**, which finally generate the open-shell product **^{1}P$_{HAT}$-i**, consisting of a tetravalent vanadium hydroxide [$VO(OH)_2$] and a methyl radical $CH_3^{\bullet}$, through homolysis of C–H bond (see Fig. 2b and Table S2†). As discussed in Section 3.1, the O_t atom of VO_2OH have zero spin density, which is hard to abstract a hydrogen atom from CH_4 through the radical HAT mechanism. Consistently, noticeable energy consumptions (38.5–42.5 kcal mol^{-1}) were found along the HAT pathways on both of the singlet and triplet PESs.

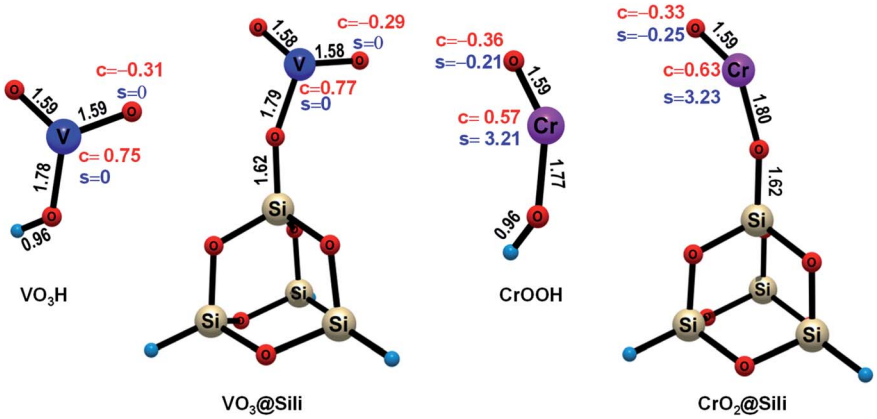

Fig. 1 The diagrams of the key bond lengths (black), the Hirshfeld charge (*c*, red) and spin density (*s*, blue) distributions for the catalyst clusters studied in this paper (the property parameters on only one side O_t of VO_2OH are labeled in this figure for clarity).

© 2021 The Author(s). Published by the Royal Society of Chemistry

Open Access Article. Published on 17 March 2021. Downloaded on 2/9/2026 10:09:49 PM.
This article is licensed under a Creative Commons Attribution-NonCommercial 3.0 Unported Licence.

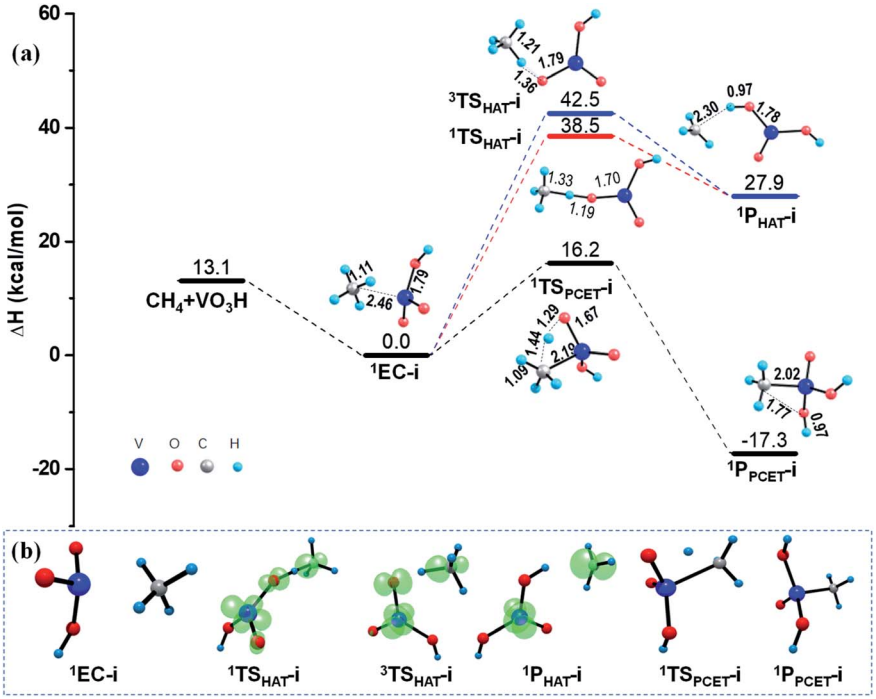

Fig. 2 (a) PESs (ΔH, kcal mol^{-1}) for the reaction of CH_4 with an unsupported VO_2OH cluster, obtained at the B3LYP-D3/ma-def2-TZVPP//B3LYP-D3/TZVP level of theory. Critical structures are given with the key bond lengths in Å. (b) The evolution of the spin density distribution along the reaction pathway.

In contrast, the C–H activation of CH_4 is relatively easy to proceed along the PCET pathway mediated by VO_2OH, by overcoming a moderate barrier of 16.4 kcal mol^{-1}, as shown in Fig. 2. In this case, the H atom is transferred as a proton from the CH_4 moiety to the terminal O_t atom of VO_2OH, forming a new O–H bond; meanwhile the generated methyl anion CH_3^- with an electron pair is transferred to the positive V center, forming a new V–C bond. This process eventually produces a relatively stable molecular structure (−17.3 kcal mol^{-1}) of **$^1P_{PCET}$-i**, without change of spin density. These calculated results suggest that the PCET mechanism is predominant for the Rxn (i) mediated by a VO_2OH cluster.

3.2.2 Rxn (ii): reaction on a silica-supported VO_3^- cluster. In the presence of silica support, the VO_3@Sili can be formed through chemisorption of VO_2OH cluster onto the silica model, and slight charge-regulation effect was observed in this case. To obtain deep understanding of the support effect on the methane C–H bond activation in Rxn (ii), we performed detailed examination of the PESs for the reaction of CH_4 with the silica supported VO_3^- cluster. As shown in Fig. 3, an encounter complex **^{1}EC-ii** is first formed when the CH_4 molecule approaches the VO_3@Sili cluster, leading to an energy decrease of 20.1 kcal mol^{-1} from the separated reactants. This means the **^{1}EC-ii** is more stable than the **^{1}EC-i**, due to the enhanced intermolecular interactions. More details can be seen from the results on SAPT energy decomposition analysis in Table S1.† Similar to the **^{1}EC-i**, there is 0.22*e* charge transferred from the CH_4 moiety to the VO_3@Sili cluster, leading to slightly polarization and initial activation of the methane molecule.

As illustrated in Fig. 3, the calculated results show negligible barrier changes of the HAT reaction paths in both singlet and triplet states, compared with the HAT reactions mediated by the free VO_2OH cluster. This is reasonable since the VO_2OH is intrinsically close-shell, and the spin density distribution is not affected in the presence of the silica support. While, for the PCET pathway, the silica support causes a larger energy barrier of 19.3 kcal mol^{-1}, producing the **$^1P_{PCET}$-ii** with −15.6 kcal mol^{-1} energy decrease. Though this cause a higher energy barrier than that in Rxn (i) from the point of view of kinetic features, both the HAT and PCET channels in Rxn (ii) are more advantageous thermodynamically due to the enhanced intermolecular interactions in the presence of silica support.

3.3 Thermal activation of CH_4 on CrOOH clusters

3.3.1 Rxn (iii): reaction on an unsupported CrOOH cluster. Sections 3.2.1 and 3.2.2 present the comparisons of different reaction pathways on different PESs for the C–H activation reaction mediated by the unsupported and supported close-shell VO_2OH clusters. In this section, we present further investigations on the thermal activation of C–H bond of methane mediated by the unsupported and silica-supported open-shell CrOOH clusters. As illustrated in Fig. 4, first, an encounter complex **^{4}EC-iii** is formed when the separated reactants CH_4 and CrOOH collide with each other, leading to an energy decrease of 1.0 kcal mol^{-1}, which is less stable compared with the **^{1}EC-i** thermodynamically. It is consistent with the results of the SAPT energy decomposition analysis, that both the electrostatic and induction interactions of the **^{4}EC-iii** are

© 2021 The Author(s). Published by the Royal Society of Chemistry

Open Access Article. Published on 17 March 2021. Downloaded on 2/9/2026 10:09:49 PM.
This article is licensed under a Creative Commons Attribution-NonCommercial 3.0 Unported Licence.

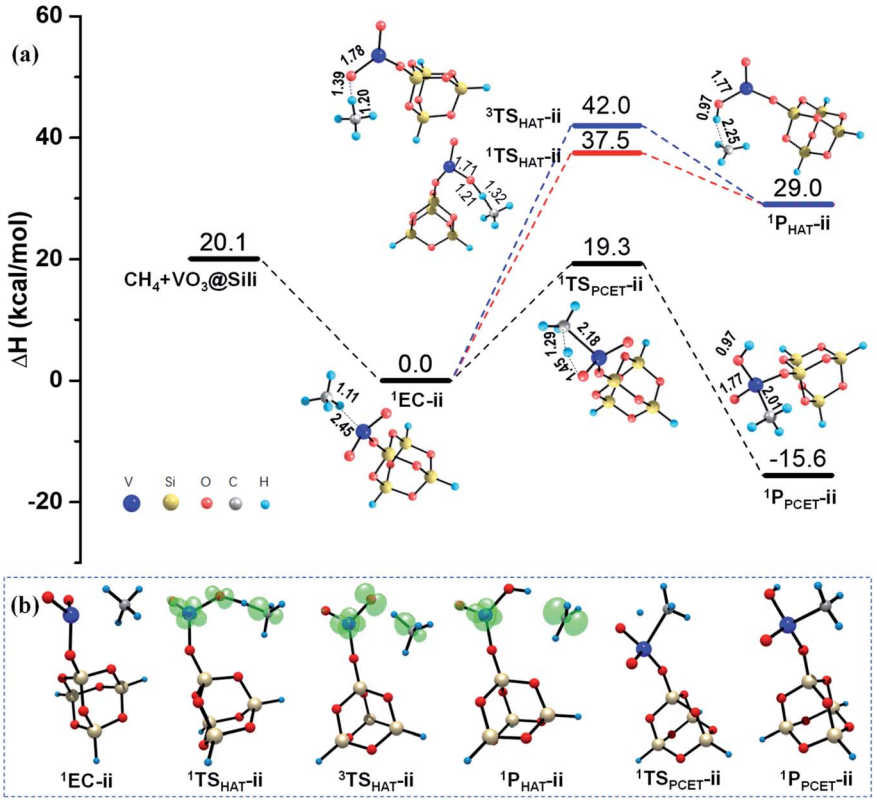

Fig. 3 (a) PESs (ΔH, kcal mol^{-1}) for the reaction of CH_4 with the silica supported VO_3^- cluster, obtained at the B3LYP-D3/ma-def2-TZVPP//B3LYP-D3/def-TZVP level of theory. Critical structures are given with the key bond lengths in Å. (b) The evolution of the spin density distribution along the reaction pathway.

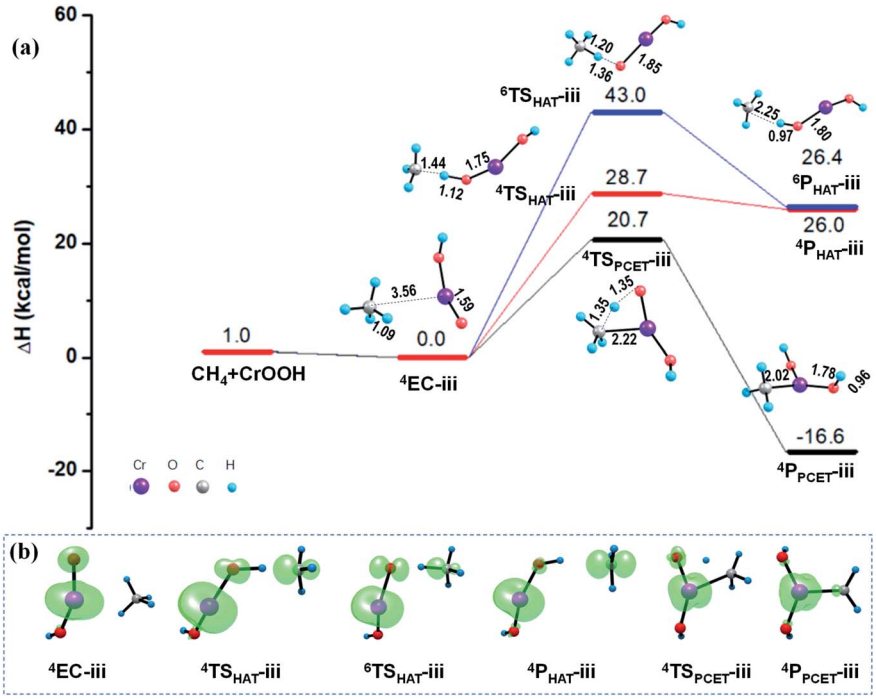

Fig. 4 (a) PESs (ΔH, kcal mol^{-1}) for the reaction of CH_4 with an unsupported CrOOH cluster, obtained at the B3LYP-D3/ma-def2-TZVPP//B3LYP-D3/def-TZVP level of theory. Critical structures are given with the key bond lengths in Å. (b) The evolution of the spin density distribution along the reaction pathway.

Open Access Article. Published on 17 March 2021. Downloaded on 2/9/2026 10:09:49 PM.
This article is licensed under a Creative Commons Attribution-NonCommercial 3.0 Unported Licence.

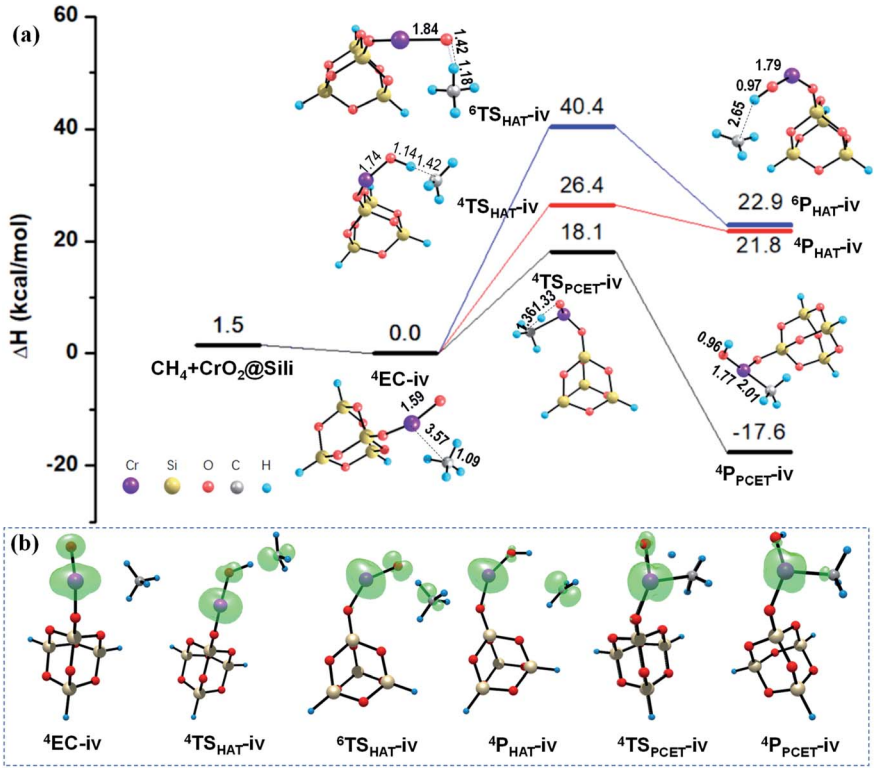

Fig. 5 (a) PESs (Δ*H*, kcal mol^{-1}) for the reaction of CH_4 with the silica supported CrO_2^- cluster, obtained at the B3LYP-D3/ma-def2-TZVPP//B3LYP-D3/def-TZVP level of theory. Critical structures are given with the key bond lengths in Å. (b) The evolution of the spin density distribution along the reaction pathway.

significantly weaker than that of the **^{1}EC-i** (see Table S1†). In consequence, only 0.01*e* is transferred from the CH_4 molecule to the CrOOH cluster (see Table S2†), and the CH_4 molecule is hardly polarized in this condition with four C–H bonds of almost equal bond length (1.09 Å). In line with expectations, a higher energy barrier of 20.7 kcal mol^{-1} (compared with the PCET path in Rxn (i)) was found computationally along the PCET path in Rxn (iii) mediated by the free CrOOH cluster. This PCET process can be described as a heterolytic cleavage of C–H bond of the methane, in which the hydrogen atom is transferred to the O_t site as a proton, and the CH_3 moiety is concertedly transferred to the Cr^{3+} site as an anion (CH_3^-). As thus, two new bonds (O_t–H and Cr–C) are formed in the product P_{PCET}, with an energy decrease of −16.6 kcal mol^{-1}.

As mentioned in Section 3.1, unlike the PCET mechanism, the O_t-center spin is necessary as a prepared site to abstract the H atom in the HAT mechanism. Different from the close-shell VO_2OH cluster, a spin density of −0.21 was found located on the terminal O_t atom of the quartet CrOOH cluster (see Fig. 4b and Table S2†). Correspondingly, the HAT reaction path in quartet state towards the methane C–H bond activation is more feasible with a smaller barrier of 28.7 kcal mol^{-1}, compared with that in the Rxn (i) (38.5 kcal mol^{-1}). The $CH_3^{\bullet}$ is then released, and the H atom is transferred to the O_t atom, forming a divalent chromium hydroxide [$Cr(OH)_2$]. However, the HAT pathways on the sextet PESs in Rxn (iii) and (iv) are both suppressed severely by the energy consumption with more than 40.0 kcal mol^{-1} barriers, due to significant electronic reorganizations are need to access the sextet transition states **^{6}TS$_{HAT}$-iii** and **^{6}TS$_{HAT}$-iv** (see Fig. 4b, 5b and Table S2†).

3.3.2 Rxn (iv): reaction on a supported CrO_2^- cluster. To explore the silica support effect on the catalytic activity of the CrOOH cluster towards the methane C–H activation, the PESs of the Rxn (iv) were inspected as shown in Fig. 5. The intermolecular interaction was also found slightly enhanced in presence of the silica support, forming the encounter complex **^{4}EC-iv** (see Table S1†). The calculated energy barrier is 18.1 kcal mol^{-1} along the PECT pathway in Rxn (iv) (Fig. 5a), which is 2.6 kcal mol^{-1} lower than that mediated by the free CrOOH cluster in Rxn (iii) (Fig. 4a). Though, the calculated negative charge located on the terminal O_t atom of CrO_2@Sili cluster is a little larger than that on the O_t atom of the free CrOOH (CrOOH: $-0.32e$ → CrO_2@Sili: $-0.36e$), which is adverse to the proton transfer to the O_t site, forming a new O_t–H bond; while we found that the silica support lead to a more positive charged Cr center (CrOOH: $0.56e$ → CrO_2@Sili: $0.62e$), which is in favor of the attack of CH_3^- to the $Cr^{\delta+}$ site, resulting in a new Cr–C bond. Thus, it can be concluded from our computational results, that the PECT mechanism is not only related to the nucleophilicity of the O_t site, but also associated with the electrophilicity of the metal center site, which is consistent with the regulation rule of Lewis acidity–basicity of the [M^+–O^-] unit reported by Schwarz *et al.*[28]

© 2021 The Author(s). Published by the Royal Society of Chemistry

Open Access Article. Published on 17 March 2021. Downloaded on 2/9/2026 10:09:49 PM.
This article is licensed under a Creative Commons Attribution-NonCommercial 3.0 Unported Licence.

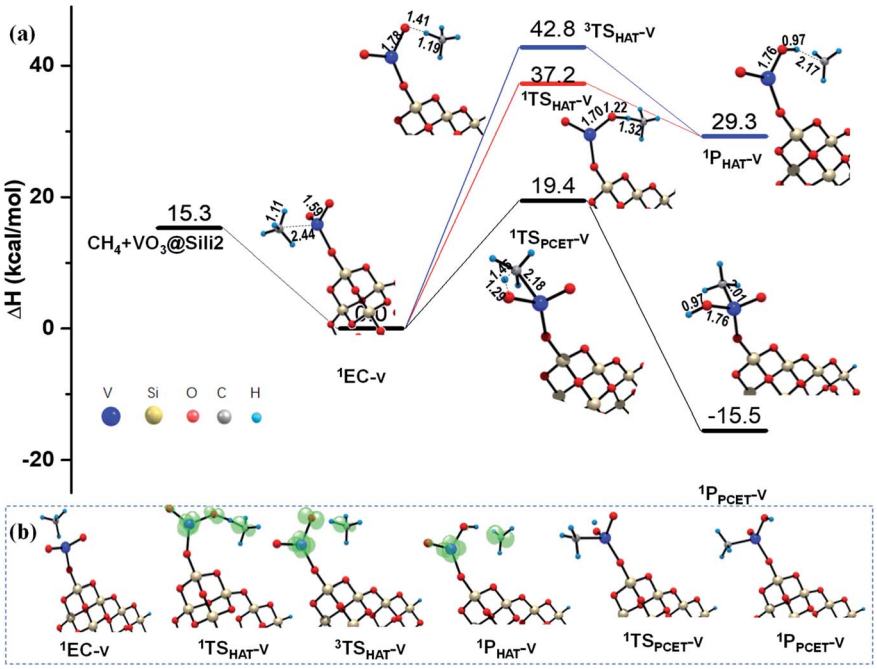

Fig. 6 (a) PESs (Δ*H*, kcal mol^{-1}) for the reaction of CH_4 with VO_3^- cluster supported by the larger $Si_{16}O_{30}H_3$ cluster, obtained at the B3LYP-D3/BSII//B3LYP-D3/BSI level of theory. Critical structures are given with the key bond lengths in Å. (b) The evolution of the spin density distribution along the reaction pathway.

As described in Section 3.1, the spin density on the O_t atom is slightly increased once the CrO_2@Sili is formed through chemisorption of the CrOOH cluster onto the silica support. The larger spin density on O_t atom means it is more facilitated to abstract a H atom from the CH_4 molecule mediated by the supported CrO_2^- cluster *versus* that in the reaction Rxn (iii) mediated by the free CrOOH cluster. As expected, a smaller barrier (26.4 kcal mol^{-1}) was found computationally along the singlet HAT pathway, which is 2.3 kcal mol^{-1} lower than that under the HAT pathway mediated by the free CrOOH in Rxn (iii). Moreover, the difference of the energy barriers along HAT paths are significantly smaller mediated by open-shell CrOOH and CrO_2@Sili (26.4–28.7 kcal mol^{-1}), than that mediated by the close-shell VO_2OH and VO_3@Sili clusters (37.5–38.5 kcal mol^{-1}), which is in line with the previous findings that the spin density at the hydrogen-acceptor site plays a crucial role for C–H bond activation proceeding by HAT mechanism. It is worth mentioning that, though the PCET mechanism was found more active than that of HAT mechanism in the four methane activation reactions (Rxn (i)–(iv)), it is not always true for different reaction systems.[51–54] For example, the HAT pathway was found more facilitated mediated by the cationic metal–carbon cluster FeC_4^+, induced by localized spin density generated *in situ* once the reactants encounter each other.[53]

3.4 Rxn (v) *vs.* Rxn (ii): investigation of silica cluster size effects

The results shown in the above sections about the silica support are based a small cluster model (Sili) containing 4 Si atoms. As is known, the metal sites are always resided on a rough surface since catalytic supports are always mesoporous materials. Furthermore, the particle size of metal or oxide clusters may possibly affect their catalytic activity, which depends on the localized or delocalized properties of the reactions toward the cluster surface.[55,56] In order to know whether the small model of Sili is representative for a catalytic support of silica, and also to understand as well the cluster size effect of the silica model used in this work toward the C–H bond activation of methane, a larger $Si_{16}O_{30}H_3$ cluster model was also examined for the reaction mediated by silica-supported VO_3^- cluster (VO_3@Sili2 in Rxn (v)). Rxn (v) differs with Rxn (ii) only in the model of the silica support.

As shown in Fig. 6, the differences of reaction barrier along the HAT reaction paths in both singlet and triplet states are within 0.6 kcal mol^{-1}, predicted by using the two silica models ($Si_{16}O_{30}H_3$ in Rxn (v) *vs.* $Si_4O_6H_3$ in Rxn (ii)). The reaction barrier along the PCET pathways in Rxn (ii) and (v) show only a small difference of 0.1 kcal mol^{-1}. The two products in Rxn (v) and (ii) also show similar thermodynamic stability with energy differences of 0.1–0.3 kcal mol^{-1}. In addition, the changes of geometries along both the HAT and PCET pathways in Rxn (v) are very close to that in Rxn (ii), by using the larger and the smaller silica cluster models. In consequence, these calculated results show that the smaller cluster model of $Si_4O_6H_3$ is as reliable as the larger one of $Si_{16}O_{30}H_3$ at least for the current research in this work.

4. Conclusion

In this work, a systematic DFT computational work have been performed to provide the mechanism comparison regarding the C–H bond activation of methane through HAT and PCET

© 2021 The Author(s). Published by the Royal Society of Chemistry

Open Access Article. Published on 17 March 2021. Downloaded on 2/9/2026 10:09:49 PM.
This article is licensed under a Creative Commons Attribution-NonCommercial 3.0 Unported Licence.

pathways mediated by the close-shell VO_2OH, the open-shell CrOOH, as well as their silica supported clusters.

For the four reactions (Rxn (i)–(iv)) examined, the HAT reaction towards methane C–H bond activation is dominated by the spin density on the O_t site, and the PCET reaction is codetermined by the nucleophilicity of the O_t site and the electrophilicity of the metal center site. Benefiting from the obvious spin density on terminal O_t atom, the calculated HAT reactions in quartet state mediated by the open-shell CrOOH and CrO_2@Sili clusters are demonstrated more favorable than that in singlet state mediated by the close-shell VO_2OH and VO_3@Sili clusters. In contrast, there are relatively smaller differences of the energy barriers through PCET mechanism among the four reactions (Rxn (i)–(iv)). Moreover, all the HAT reactions examined are disadvantaged compared with the PCET pathways, note that the products obtained under the PCET mechanism should suffer further M(V, Cr)–C bond cleavage to generate the free $CH_3^{\bullet}$ radical. In the presence of silica support, the intermolecular interaction between the CH_4 molecule and the catalyst cluster is enhanced, especially for the reactions mediated by VO_2OH cluster, leading to the C–H bond activation of methane being more thermodynamically feasible.

Conflicts of interest

There are no conflicts to declare.

Acknowledgements

Support from the National Natural Science Foundation of China (21576291), and Shandong Province Natural Science Foundation (ZR2014BM002) is gratefully acknowledged.

References

1 P. Tang, Q. Zhu, Z. Wu and D. Ma, *Energy Environ. Sci.*, 2014, **7**, 2580–2591.
2 A. Caballero and P. J. Pérez, *Chem. Soc. Rev.*, 2013, **42**, 8809–8820.
3 K. Otsuka and Y. Wang, *Appl. Catal., A*, 2001, **222**, 145–161.
4 R. Horn and R. Schloegl, *Catal. Lett.*, 2015, **145**, 23–39.
5 C. Karakaya and R. J. Kee, *Prog. Energy Combust. Sci.*, 2016, **55**, 60–97.
6 Y. Liu, D. Deng and X. Bao, *Chem*, 2020, **6**, 2497–2514.
7 S. J. Blanksby and G. B. Ellison, *Acc. Chem. Res.*, 2003, **36**, 255–263.
8 N. J. Gunsalus, A. Koppaka, S. H. Park, S. M. Bischof, B. G. Hashiguchi and R. A. Periana, *Chem. Rev.*, 2017, **117**, 8521–8573.
9 X. Meng, X. Cui, N. P. Rajan, L. Yu, D. Deng and X. Bao, *Chem*, 2019, **5**, 2296–2325.
10 U. Zavyalova, M. Holena, R. Schloegl and M. Baerns, *ChemCatChem*, 2011, **3**, 1935–1947.
11 H. Schwarz, *Isr. J. Chem.*, 2015, **54**, 1413–1431.
12 M. G. Quesne, F. Silveri, N. H. D. Leeuw and R. R. A. Catlow, *Front. Chem.*, 2019, **7**, 182.
13 H. Schwarz, S. Shaik and J. Li, *J. Am. Chem. Soc.*, 2017, **139**, 17201–17212.
14 Y. X. Zhao, X. N. Li, Z. Yuan, Q. Y. Liu, Q. Shi and S. G. He, *Chem. Sci.*, 2016, **7**, 4730–4735.
15 C. Geng, T. Weiske, J. Li, S. Shaik and H. Schwarz, *J. Am. Chem. Soc.*, 2018, **141**, 599–610.
16 H. F. Li, Z. Y. Li, Q. Y. Liu, X. N. Li, Y. X. Zhao and S. G. He, *J. Phys. Chem. Lett.*, 2015, **6**, 2287–2291.
17 B. A. Peter, *Chem.–Eur. J.*, 2017, **23**, 10–18.
18 Y. X. Zhao, Z. Y. Li, Y. Yang and S. G. He, *Acc. Chem. Res.*, 2018, **51**, 2603–2610.
19 X. Lin, Y. Xi and J. Sun, *J. Phys. Chem. C*, 2012, **116**, 3503–3516.
20 G. Fu, X. Xu, X. Lu and H. Wan, *J. Am. Chem. Soc.*, 2005, **127**, 3989.
21 B. Xing, X. Y. Pang and G. C. Wang, *J. Catal.*, 2011, **282**, 74–82.
22 B. Xing and G. C. Wang, *Phys. Chem. Chem. Phys.*, 2014, **16**, 2621–2629.
23 Y. Q. Wang, C. Q. Lv and G. C. Wang, *RSC Adv.*, 2015, **5**, 66221–66230.
24 J. J. Varghese, Q. T. Trinh and S. H. Mushrif, *Catal. Sci. Technol.*, 2016, **6**, 3984–3996.
25 D. Hibbitts and M. Neurock, *Surf. Sci.*, 2016, **650**, 210–220.
26 J. Wang and G. C. Wang, *J. Phys. Chem. C*, 2018, **122**, 17338–17346.
27 N. Dietl, M. Schlangen and H. Schwarz, *Angew. Chem., Int. Ed.*, 2012, **51**, 5544–5555.
28 J. Li, S. Zhou, J. Zhang, M. Schlangen, D. Usharani, S. Shaik and H. Schwarz, *J. Am. Chem. Soc.*, 2016, **138**, 11368–11377.
29 J. L. Li, S. D. Zhou, M. Schlangen, T. Weiske and H. Schwarz, *Angew. Chem., Int. Ed.*, 2016, **128**, 13266–13269.
30 S. Feyel, J. Dobler, D. Schroder, J. Sauer and H. Schwarz, *Angew. Chem., Int. Ed.*, 2006, **45**, 4681–4685.
31 R. C. Bell and A. W. Castleman Jr, *J. Phys. Chem. A*, 2002, **106**, 9893–9899.
32 X. Xu, F. Faglioni and W. A. Goddard III, *J. Phys. Chem. A*, 2002, **106**, 7171–7176.
33 P. Serna and B. C. Gates, *Acc. Chem. Res.*, 2014, **47**, 2612–2620.
34 Y. Xi, B. Chen, X. Lin, H. Fu and C. Wang, *Comput. Theor. Chem.*, 2016, **1076**, 65–73.
35 M. J. Frisch, *et al.Gaussian 09, Revision B. 01*, Gaussian, Inc., Wallingford, 2010.
36 A. D. Becke and D. Axel, *J. Chem. Phys.*, 1993, **98**, 1372–1377.
37 C. Lee, W. Yang and R. G. Parr, *Phys. Rev. B: Condens. Matter Mater. Phys.*, 1988, **37**, 785–789.
38 P. J. Stephens, F. J. Devlin, C. F. Chabalowski and M. J. Frisch, *J. Phys. Chem.*, 1994, **98**, 247–257.
39 S. Grimme, J. Antony, S. Ehrlich and H. Krieg, *J. Chem. Phys.*, 2010, **132**, 154104.
40 M. Dolg, U. Wedig, H. Stoll and H. Preuss, *J. Chem. Phys.*, 1987, **86**, 866–872.
41 A. Schäfer, C. Huber and R. Ahlrichs, *J. Chem. Phys.*, 1994, **100**, 5829–5835.
42 K. Eichkorn, F. Weigend, O. Treutler and R. Ahlrichs, *Theor. Chem. Acc.*, 1997, **97**, 119–124.

© 2021 The Author(s). Published by the Royal Society of Chemistry

Open Access Article. Published on 17 March 2021. Downloaded on 2/9/2026 10:09:49 PM.
This article is licensed under a Creative Commons Attribution-NonCommercial 3.0 Unported Licence.

43 K. Fukui, *Acc. Chem. Res.*, 1981, **14**, 363–368.
44 H. P. Hratchian and H. B. Schlegel, *J. Chem. Phys.*, 2004, **120**, 9918–9924.
45 J. M. L. Martin and A. Sundermann, *J. Chem. Phys.*, 2001, **114**, 3408.
46 F. Weigend and R. Ahlrichs, *Phys. Chem. Chem. Phys.*, 2005, **7**, 3297–3305.
47 J. Zheng, X. Xu and D. G. Truhlar, *Theor. Chem. Acc.*, 2011, **128**, 295–305.
48 F. L. Hirshfeld, *Theor. Chim. Acta*, 1977, **44**, 129–138.
49 T. Lu and F. Chen, *J. Comput. Chem.*, 2012, **33**, 580–592.
50 J. M. Turney, A. C. Simmonett, R. M. Parrish, E. G. Hohenstein, F. A. Evangelista, J. T. Fermann, B. J. Mintz, L. A. Burns, J. J. Wilke and M. L. Abrams, *Wiley Interdiscip. Rev.: Comput. Mol. Sci.*, 2012, **2**, 556–565.
51 W. Lai, C. Li, P. D. H. Chen and P. D. S. Shaik, *Angew. Chem., Int. Ed.*, 2012, **51**, 5556–5578.
52 S. Ye and F. Neese, *Proc. Natl. Acad. Sci. U. S. A.*, 2011, **108**, 1228–1233.
53 C. Geng, J. Li, T. Weiske and H. Schwarz, *Chem.–Eur. J.*, 2019, **25**, 12940–12945.
54 X.-L. Ding, X.-N. Wu, Y.-X. Zhao and S.-G. He, *Acc. Chem. Res.*, 2012, **45**, 382–390.
55 C. S. Cooper, R. J. Oldmana and C. R. A. Catlowb, *Chem. Commun.*, 2015, **51**, 5856–5859.
56 Z. Hu and C. H. Turner, *J. Am. Chem. Soc.*, 2007, **129**, 3863–3878.

© 2021 The Author(s). Published by the Royal Society of Chemistry